EARTHQUAKE ENGINEERING AND STRUCTURAL DYNAMICS, VOL. 25, 465–481 (1996)

SEISMIC GROUND MOTION SYNTHETICS OF THE 1989 LOMA PRIETA EARTHQUAKE

RUICHONG ZHANG * AND GEORGE DEODATIS †
Department of Civil Engineering and Operations Research, Princeton University, Princeton, NJ 08544, U.S.A.

SUMMARY

A discrete wave number approach in conjunction with a propagator-based formalism is used to synthesize the Loma Prieta earthquake ground motion at both the near and the far field, taking into account all kinds of seismic waves (body and surface). A bilaterally propagating shear slip over a rectangular fault is used to describe the seismic source mechanism, while the earth model is based on geological profiles of the Santa Cruz mountain area and consists of three layers overlaying a half-space. The synthesized ground motion is first compared with actual records from the Loma Prieta earthquake and the agreement between the two is found to be satisfactory, as far as magnitude, duration and essential wave form characteristics are concerned. Then, ground motions are synthesized and plotted at a dense grid of observer locations over a large area around the epicenter, at different time instants. Using such plots, it is possible to study the generation and propagation of different kinds of seismic waves, the spatial variability of ground motion, as well as the development of the permanent ground deformation.

KEY WORDS: ground motion synthetics; discrete wave number approach; Loma Prieta earthquake; near–field ground motion; seismic waves; spatial variability of ground motion

INTRODUCTION

The magnitude 7·1 Loma Prieta earthquake struck the San Francisco Bay area on 17 October 1989 and ruptured a 40 km segment of the San Andreas fault in the southern Santa Cruz Mountains of northern California. The hypocenter of the main shock was located at a depth of 17·6 km.[1] The earthquake caused 62 direct fatalities and over $6 billion in property damage over a widespread area. It is therefore obvious that modelling and synthesizing the Loma Prieta strong ground motion over a large area around the epicenter is of paramount importance to the earthquake-resistant design of structures in northern California.

The theory of generation of seismic waves at a dislocation-type seismic source and their subsequent propagation through a layered half-space has been well developed during the last three decades. This theory has been applied both by seismologists and engineers to synthesize earthquake ground motion. References 2–23 are representative works in this area. Specifically for the Loma Prieta earthquake, the description of the seismic source mechanism and the modelling of ground motion have been examined, among others, by: Wald *et al.*,[24] Beroza,[25] Fletcher and Boatwright[26] and Chin and Aki.[27] Recently, Zeng *et al.*[28,29] estimated the slip distribution over an assumed rectangular fault for the Loma Prieta earthquake using ray theory and near field earthquake records (specifically, 14 observation sites were considered inside a circular region of 35 km radius around the epicenter). It should be noted that only direct arrivals of S-waves were taken into account by Zeng *et al.*,[28,29] for the sake of convenience and simplicity of computations. However, the results obtained through such an approach are acceptable from the engineering point of view, because S-waves dominate the seismic wave energy in the near field, compared to P-waves and non-direct body waves. In addition, surface waves are not well developed in the near field. At this juncture, it should

* Research Associate
† Assistant Professor

CCC 0098–8847/96/050465–17
© 1996 by John Wiley & Sons, Ltd.
Received 22 September 1994
Revised 1 December 1995

be pointed out that the methodology used by Zeng *et al.*[28, 29] is not suitable to synthesize the far-field ground motion, because it is not taking into account the surface waves which are dominant in the far field.

In this paper, a discrete wave number approach in conjunction with a propagator-based formalism is used to synthesize the Loma Prieta earthquake ground motion at both the near and the far field. A bilaterally propagating shear slip over a rectangular fault[29] is used to describe the seismic source mechanism in the present study. The earth model is based on geological profiles of the Santa Cruz mountain area[30] and consists of three layers overlaying a half-space. The synthesized ground motion is compared with actual records from the Loma Prieta earthquake.

The discrete wave number approach used in this paper in conjunction with a propagator-based formalism to synthesize earthquake ground motion is an extension of the methodology developed in References 31–33. It should be mentioned that the development of this methodology was based on the work of Bouchon,[9] Chouet[20] and Dunkin.[34] The approach proposed in this paper has two important advantages. First, it takes into account all kinds of seismic waves (body and surface) and second, it yields the ground motions at a dense grid of observer locations on the ground surface.

FORMULATION

The ground is assumed to consist of a number of flat layers that are overlaying a half-space. Each one of the layers, as well as the half-space, is characterized by a P-wave velocity, a S-wave velocity, a rigidity and an attenuation factor as defined by Aki and Richards.[11]

The seismic source is modelled by a slip distribution of arbitrary orientation over a fault of rectangular shape (note that, in general, the fault can have an arbitrary shape). As shown in Figure 1, the fault orientation is defined by the strike ϕ_s $[0, 2\pi)$ and the dip δ $[0, \pi/2]$. ϕ_s is measured clockwise from the north direction and δ is measured down from the horizontal. The slip direction is defined by the rake λ $[-\pi, \pi]$ which is the angle within the fault plane between the strike direction and the slip.[11] Since a pure strike-slip corresponds to $\lambda = 0$ or π and a pure dip-slip to $\lambda = -\pi/2$ or $\pi/2$, a slip of arbitrary orientation can be decomposed into pure strike-slip and pure dip-slip components.

Without any loss of generality, the co-ordinate system is selected so that the (x, y) plane coincides with the horizontal ground surface, the x-direction coincides with the strike direction and the z-direction with the increasing depth direction, as shown in Figure 1.

The seismic fault is then discretized into a number of subfaults and the slip on each subfault is modelled by a double couple acting at the centre of the subfault area. The earthquake ground motion is therefore obtained from the superposition of a number of double couples which are distributed evenly over the seismic fault area. Each one of these double couples is characterized by a different final slip and is triggered at a different time instant. According to this discretization, the displacement field at the ground surface can be expressed as

$$U_n(x, y, t) = \sum_{i=1}^{N} U_n^{(i)}(x, y, t; x_i, y_i, z_i, t_i); \quad n = x, y, z \tag{1}$$

where subscript n indicates the displacement component, N is the total number of double couples in the discretization of the seismic fault and $U_n^{(i)}(x, y, t; x_i, y_i, z_i, t_i)$ denotes the displacement at the ground surface caused by the ith double couple acting at point (x_i, y_i, z_i) and triggered at time instant t_i. As mentioned earlier, a slip of arbitrary orientation can be decomposed into pure strike-slip and pure dip-slip components. Accordingly, the corresponding displacement can be expressed as the summation of two terms: one due to the pure strike-slip component of the slip and the other due to the pure dip-slip component of the slip. Consequently, $U_n^{(i)}$ appearing in equation (1) can be written as

$$U_n^{(i)}(x, y, t; x_i, y_i, z_i, t_i) = U_n^{s^{(i)}}(x, y, t; x_i, y_i, z_i, t_i) + U_n^{d^{(i)}}(x, y, t; x_i, y_i, z_i, t_i) \tag{2}$$

where superscripts s and d refer to the strike-slip and the dip-slip, respectively.

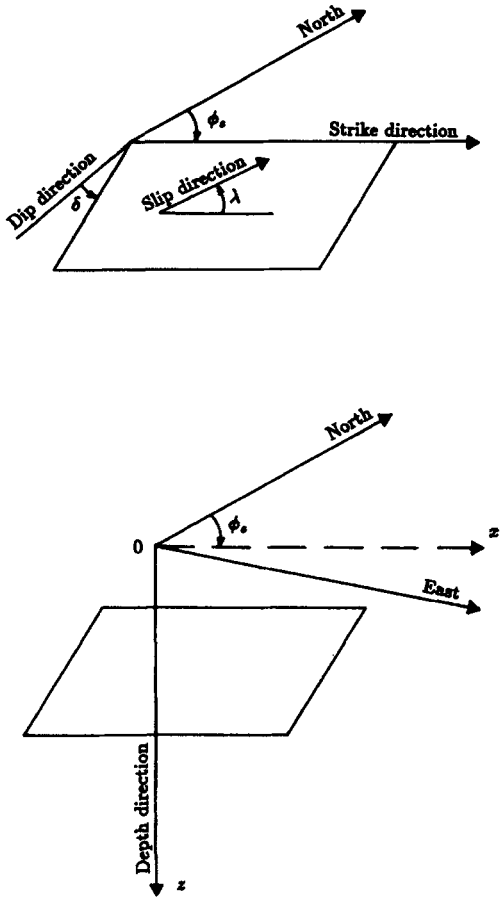

Figure 1. Fault orientation

In Theoharis and Deodatis,[32] it was shown that the displacement fields $U_n^{s^{(i)}}$ and $U_n^{d^{(i)}}$ can be expressed as

$$U_n^{s^{(i)}}(x,y,t;x_i,y_i,z_i,t_i) = M_{xy}^{(i)}(t-t_i) * G_n^1(x,y,t;x_i,y_i,z_i) + M_{xz}^{(i)}(t-t_i) * G_n^2(x,y,t;x_i,y_i,z_i) \tag{3}$$

$$U_n^{d^{(i)}}(x,y,t;x_i,y_i,z_i,t_i) = M_{yy}^{(i)}(t-t_i) * G_n^3(x,y,t;x_i,y_i,z_i) + M_{zz}^{(i)}(t-t_i) * G_n^4(x,y,t;x_i,y_i,z_i) + M_{yz}^{(i)}(t-t_i) * G_n^5(x,y,t;x_i,y_i,z_i) \tag{4}$$

where $M_{\zeta_1\zeta_2}^{(i)}(\zeta_1,\zeta_2 = x,y,z)$ are the time-dependent components of the seismic moment tensor associated with the ith double couple, $*$ is the convolution symbol and G_n^j; $j = 1, 2, \ldots, 5$ are expressions involving partial derivatives of the displacement field due to unidirectional unit impulses applied at point (x_i, y_i, z_i), with respect to the coordinates of this same point (refer to Reference 32).

Equations (3) and (4) are then transformed into the frequency-wave number domain:

$$\tilde{U}_n^{s^{(i)}}(\kappa_x,\kappa_y,\omega;x_i,y_i,z_i,t_i) = \tilde{M}_{xy}^{(i)}(\omega;t_i)\tilde{G}_n^1(\kappa_x,\kappa_y,\omega;x_i,y_i,z_i) + \tilde{M}_{xz}^{(i)}(\omega;t_i)\tilde{G}_n^2(\kappa_x,\kappa_y,\omega;x_i,y_i,z_i) \tag{5}$$

$$\tilde{U}_n^{d^{(i)}}(\kappa_x,\kappa_y,\omega;x_i,y_i,z_i,t_i) = \tilde{M}_{yy}^{(i)}(\omega;t_i)\tilde{G}_n^3(\kappa_x,\kappa_y,\omega;x_i,y_i,z_i) + \tilde{M}_{zz}^{(i)}(\omega;t_i)\tilde{G}_n^4(\kappa_x,\kappa_y,\omega;x_i,y_i,z_i) + \tilde{M}_{yz}^{(i)}(\omega;t_i)\tilde{G}_n^5(\kappa_x,\kappa_y,\omega;x_i,y_i,z_i) \tag{6}$$

where κ_x and κ_y are wave numbers, ω is the frequency and a tilde denotes a Fourier-transformed quantity. Closed-form analytic expressions for the $\tilde{G}_n^j$; $j = 1,2,\ldots,5$ can be found in Reference 35.

Referring to equations (3)–(6), it is reminded that a displacement field $U(x,y,t)$ in the time–space domain is describing a propagating wave and is related to its Fourier transform $\tilde{U}(\kappa_x,\kappa_y,\omega)$ in the frequency-wave number domain through the following transformation:

$$U(x,y,t) = \int_{-\infty}^{\infty}\int_{-\infty}^{\infty}\int_{-\infty}^{\infty} \tilde{U}(\kappa_x,\kappa_y,\omega)\exp[-\mathrm{i}\kappa_x x - \mathrm{i}\kappa_y y + \mathrm{i}\omega t]\,\mathrm{d}\kappa_x\,\mathrm{d}\kappa_y\,\mathrm{d}\omega \tag{7}$$

while the inverse transformation is given by

$$\tilde{U}(\kappa_x,\kappa_y,\omega) = \frac{1}{(2\pi)^3}\int_{-\infty}^{\infty}\int_{-\infty}^{\infty}\int_{-\infty}^{\infty} U(x,y,t)\,\exp\,[\mathrm{i}\kappa_x x + \mathrm{i}\kappa_y y - \mathrm{i}\omega t]\,\mathrm{d}x\,\mathrm{d}y\,\mathrm{d}t \tag{8}$$

The time-dependent seismic moment tensor associated with the ith double couple (or equivalently with the ith subfault) is expressed as[11]

$$M_{xy}^{(i)}(t-t_i) = M^{(i)}\sin(\delta)\cos(\lambda)\,F(t-t_i) \tag{9}$$

$$M_{xz}^{(i)}(t-t_i) = -M^{(i)}\cos(\delta)\cos(\lambda)\,F(t-t_i) \tag{10}$$

$$M_{yy}^{(i)}(t-t_i) = -M^{(i)}\sin(2\delta)\sin(\lambda)\,F(t-t_i) \tag{11}$$

$$M_{yz}^{(i)}(t-t_i) = M^{(i)}\cos(2\delta)\sin(\lambda)\,F(t-t_i) \tag{12}$$

$$M_{zz}^{(i)}(t-t_i) = M^{(i)}\sin(2\delta)\sin(\lambda)\,F(t-t_i) \tag{13}$$

where δ is the dip, λ is the rake, F is a function describing the time-dependence of the moment tensor and $M^{(i)}$ is the magnitude of the seismic moment given by

$$M^{(i)} = \mu A^{(i)}\,\overline{\Delta u_i^F} \tag{14}$$

where μ is the rigidity of the medium surrounding the fault, $A^{(i)}$ is the area of the ith subfault and $\overline{\Delta u_i^F}$ is the average final slip on the ith subfault.

The Fourier-transformed expressions of the components of the seismic moment tensor shown in equations (9)–(13) in the frequency domain are easily obtained considering the following relation:

$$\int_{-\infty}^{\infty} F(t-t_i)\exp[-\mathrm{i}\omega t]\;\mathrm{d}t = \tilde{F}(\omega)\exp[-\mathrm{i}\omega t_i] \tag{15}$$

where $\tilde{F}(\omega)$ is the Fourier transform of $F(t)$.

Then, the complex Fourier amplitudes in the frequency-wave number domain of the displacement field on the ground surface are obtained by summing up the contributions of all N double couples:

$$\tilde{U}_n(\kappa_x,\kappa_y,\omega) = \sum_{i=1}^{N}\left[\tilde{U}_n^{s^{(i)}}(\kappa_x,\kappa_y,\omega;x_i,y_i,z_i,t_i) + \tilde{U}_n^{d^{(i)}}(\kappa_x,\kappa_y,\omega;x_i,y_i,z_i,t_i)\right] \tag{16}$$

where $\tilde{U}_n^{s^{(i)}}$ and $\tilde{U}_n^{d^{(i)}}$ are given in equations (5) and (6), respectively. The corresponding Fourier amplitudes of the velocity and acceleration fields can be obtained by multiplying $\tilde{U}_n(\kappa_x,\kappa_y,\omega)$ by $\mathrm{i}\omega$ and $-\omega^2$, respectively.

Finally, the displacement, velocity and acceleration fields in the space–time domain on the ground surface are obtained by performing numerically a triple Fourier transform of the corresponding frequency-wave number domain complex Fourier amplitudes.

VERIFICATION

The accuracy of the proposed discrete wave number approach to synthesize earthquake ground motion (presented in the previous section) is checked by comparing its results for a simple problem to the corresponding results by Archuleta and Hartzell.[36] It should be pointed out that Archuleta and Hartzell[36] followed an approach to calculate the displacement field which is different from the one proposed in this paper. The simple problem examined in their paper is described in the following.

The earth model is a uniform half-space with P-wave velocity $c_p = 5{\cdot}2$ km/sec, S-wave velocity $c_s = 3{\cdot}0$ km/sec, rigidity $\mu = 3 \times 10^{10}$ N/m^2 and attenuation factor $Q = 100$. The seismic source is a vertical ($\delta = \pi/2$) circular fault, having only a pure strike-slip component ($\lambda = 0$). The co-ordinates of the centre of this circular fault are $x_0 = 0$, $y_0 = 0$, $z_0 = 7$ km and its radius is $r_0 = 5$ km. The slip Δu at a distance r from the centre of the fault ($r \leqslant r_0$) and at time t is given by

$$\Delta u(r,t) = C\sigma_E \frac{c_s}{\mu} \sqrt{t^2 - \frac{r^2}{v^2}}\, H\left(t - \frac{r}{v}\right); \quad t < t_c(r) \tag{17}$$

$$\Delta u(r,t) = C\sigma_E \frac{c_s}{\mu} \sqrt{t_c(r)^2 - \frac{r^2}{v^2}}; \quad t > t_c(r) \tag{18}$$

where

$$t_c(r) = \frac{r_0}{v} + \frac{r_0 - r}{v_h} \tag{19}$$

In equations (17)–(19), C is a constant depending on the S-wave velocity c_s and on the rupture velocity v, σ_E is the effective stress, v_h is the healing velocity, μ is the rigidity of the half-space and H denotes Heaviside's step function. It is noted that the fault starts to rupture from its center at time $t = 0$. The following values are used for the parameters appearing in equations (17)–(19): $C = 0{\cdot}81$, $\sigma_E = 10^7$ N/m^2, $v = 2{\cdot}7$ km/sec and $v_h = 3{\cdot}0$ km/sec. The circular fault is discretized into $N = 76$ subfaults of approximately equal area, as described in the previous section. Finally, the triple Fourier transform of the frequency-wave number Fourier amplitudes of the displacement field [see equation (16)] to the space–time domain is performed numerically, using the Fast Fourier Transform (FFT) technique with 256×256 wave numbers and 128 frequencies.

Figure 2(a) displays the three components of the displacement at an observation site on the ground surface with coordinates $x = 3$ km, $y = 5{\cdot}2$ km, $z = 0$ obtained using the proposed discrete wave number approach, while Figure 2(b) displays the corresponding time histories obtained by Archuleta and Hartzell.[36] Although Archuleta and Hartzell used a much larger number of effective point sources ($N = 7722$ versus $N = 76$ used by the proposed discrete wave number approach), the displacement time histories of the two approaches compare extremely well, as can be seen in Figure 2. The minor differences observed in Figure 2 are due to the different number of effective point sources considered and to the different numerical techniques used by the two approaches.

SYNTHETICS OF LOMA PRIETA EARTHQUAKE

The proposed discrete wave number approach will be used now to synthesize the displacement field of the 1989 Loma Prieta earthquake.

The earth model is based on geological profiles of the Santa Cruz mountain area[30] and consists of three layers overlaying a half-space with properties shown in Table I (it should be noted that the interface between the third layer and the half-space is the Moho discontinuity). The seismic source mechanism is suggested by Zeng *et al.*[29] and consists of a bilaterally propagating shear slip over a rectangular fault. The fault has a length of 40 km along the strike direction ($\phi_s = 130°$) and a width of 14 km along the dip direction ($\delta = 70°$). Figure 3 displays rupture initiation contours at $0{\cdot}5$ sec time intervals on the 40 km × 14 km rectangular fault. The rupture process starts at point E of side AB of the fault (see Figure 3),

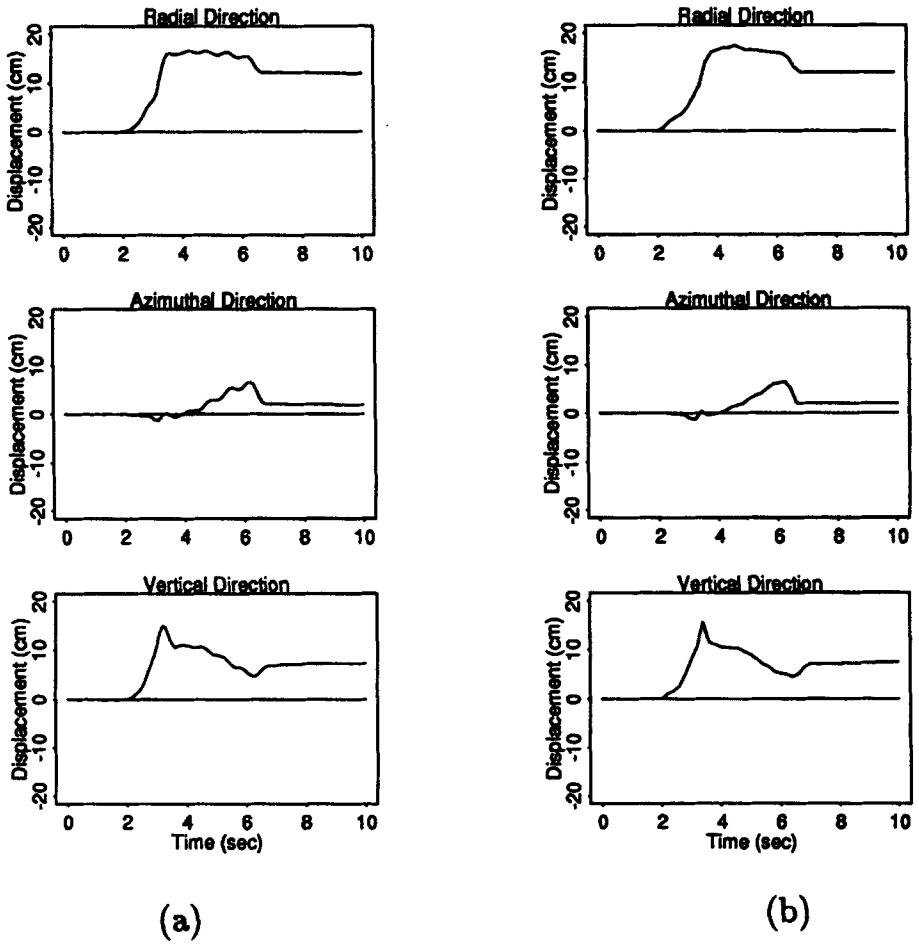

Figure 2. Three components of displacement at an observation site on the ground surface obtained for a simple problem (a) by the proposed discrete wave number approach, (b) by Archuleta and Hartzell[36]

Table I. Properties of three layers and half-space (Loma Prieta Earthquake)

	Top (first) layer	Second layer	Third layer	Half-space
Density (kg/m^3)	2046	2558	2964	3100
P-Wave velocity (m/sec)	1730	4290	6320	8000
S-Wave velocity (m/sec)	1000	2480	3649	4619
Attenuation factor	100	250	400	600
Thickness of layer (km)	0·0–0·5	0·5–3·0	3·0–25	25–∞

which is located at a depth of 17·6 km. The final values of the pure strike-slip and dip-slip components of the slip are plotted in Figure 4. At this point it should be noted that Figures 3 and 4 are plotted using data provided by Zeng *et al.*[29] The time-dependence of the slip [function $F(t)$ in equations (9)–(13)] is assumed to be a ramp function with rise time equal to 0·2 sec[29] at every point on the rectangular fault. The total seismic moment is $2{\cdot}9 \times 10^{19}$ N m. The 40 km × 14 km rectangular fault is discretized into $N = 40 \times 14 = 560$ subfaults, each having an area of 1 km^2. Finally, the triple Fourier transform of the frequency-wave number Fourier amplitudes of the displacement field [see equation (16)] to the space–time domain is performed numerically, using the FFT technique with 512×512 wave numbers and 1024 frequencies.

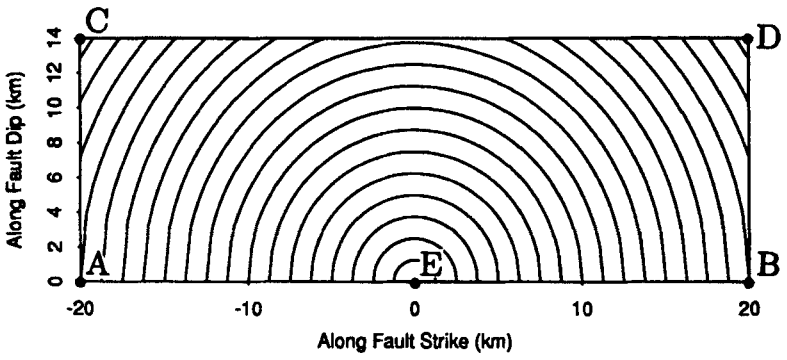

Figure 3. Rupture initiation contours at 0·5 sec time intervals on the rectangular fault (rupture starts at point E)

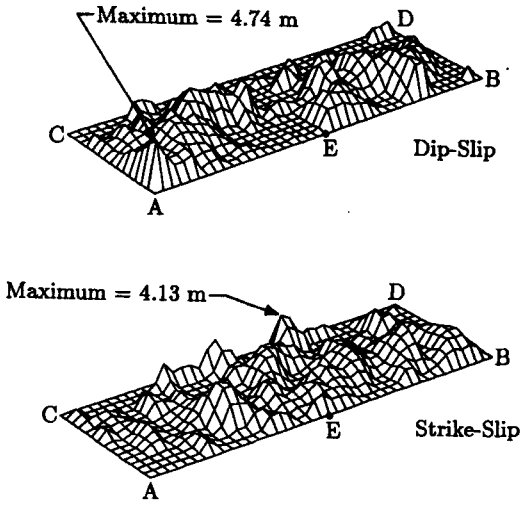

Figure 4. Final values of the pure strike-slip and dip-slip components of the slip over the rectangular fault (points A,B,C,D,E are defined in Figure 3)

In order to compare the synthesized ground motion with actual records of the Loma Prieta earthquake, the four observation sites shown in Table II are selected. The synthesized displacement time histories at these four sites are displayed in Figures 5–7. An interesting attribute of these time histories is that there is no ground motion before the arrival of the first P-wave. For example, the arrival time of the first P-wave at Watsonville (epicentral distance = 18·1 km according to Table II) can be quickly estimated as: $(\sqrt{18\cdot1^2+(17\cdot6-3\cdot0)^2}\,\text{km})/(6\cdot32\,\text{km/sec})+(3\cdot0-0\cdot5\,\text{km})/(4\cdot29\,\text{km/sec})+(0\cdot5\,\text{km})/(1\cdot73\,\text{km/sec})=4\cdot55\,\text{sec}$, where the first term in this summation represents the time the P-wave travels from point E in Figure 3 to the point on the interface between the third and the second layer directly beneath the Watsonville observation site, while the second and the third terms are the times the P-wave travels vertically through the second and the first (top) layer, respectively. This 4·55 sec time interval with no ground motion before the arrival of the first P-wave at Watsonville is easily identified in Figures 5–7. Similar time intervals with no ground motion can be readily identified for the remaining three observation sites. Another interesting attribute of the displacement time histories shown in Figures 5–7 is the estimation of the permanent (static) ground deformation after all propagating waves have passed from the observation sites. It should be noted that the amplitudes of both the propagating waves and the permanent ground deformation depend obviously on the distance of the observation site from the seismic source.

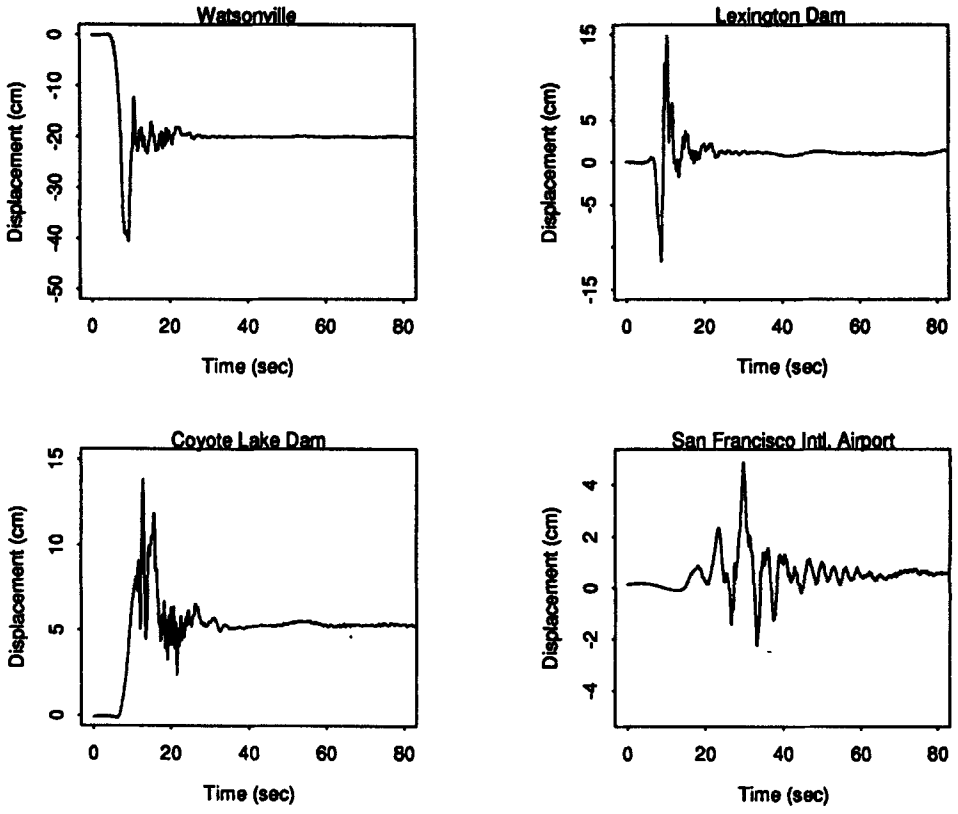

Figure 5. Synthesized displacement time histories in the strike direction (x-direction) at the four observation sites

Table II. Observation sites (Loma Prieta Earthquake)

Observation site	Epicentral distance (km)	Clockwise angle from strike direction
Watsonville	18·1	11·4°
Lexington Dam	19·2	112·3°
Coyote Lake Dam	31·0	−58·2°
San Francisco Intl. Airport	79·2	−165·0°

At this stage, it is not possible to compare directly the displacement time histories shown in Figures 5–7 with the corresponding actual records of the Loma Prieta earthquake. This is due to two reasons. The first one is the inadequacy of currently available instruments to record ground motion at relatively low frequencies, while the second one is the numerical difficulty of the proposed discrete wave number approach to synthesize ground motion at relatively high frequencies. In order to overcome this problem, both the synthesized and recorded displacement time histories at the four observation sites are filtered out of frequencies smaller than 0·3 Hz and larger than 2 Hz. Then, synthesized and recorded displacement time histories are plotted together for comparison purposes in Figures 8–11. Although there are differences between synthesized and recorded time histories in Figures 8–11, a careful study reveals reasonably good agreement in magnitude, duration and essential wave form characteristics. It is therefore justified to use the proposed discrete wave number approach in conjunction with the adopted earth and seismic source models to synthesize the Loma Prieta earthquake ground motion.

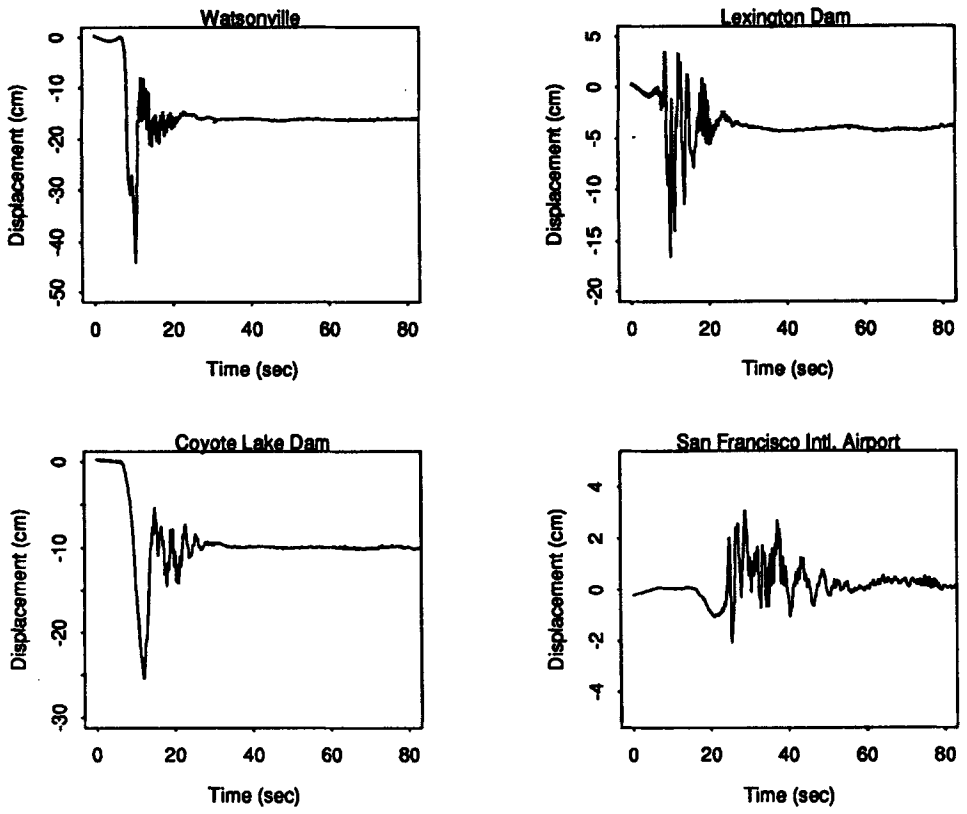

Figure 6. Synthesized displacement time histories in the direction perpendicular to the strike (y-direction) at the four observation sites

As mentioned in the introduction, a unique advantage of the proposed discrete wave number approach is that ground motions can be synthesized at a dense grid of observer locations on the ground surface. This is demonstrated in Figure 12, where the displacement field in the strike direction (x-direction) is plotted over a 480 km×480 km area around the epicenter at six time instants (the displacement field is synthesized at 1024 time instants, but only six are displayed here because of space limitations). The generation and propagation of different kinds of seismic waves, the spatial variability of ground motion, as well as the development of the permanent (static) ground deformation, can be examined by carefully studying such plots. Finally, it should be pointed out one more time that all kinds of seismic waves (body and surface) are present in the displacement fields shown in Figure 12.

POTENTIAL ENGINEERING APPLICATIONS

The discrete wave number approach in conjunction with a propagator-based formalism presented in this paper can be used to synthesize earthquake ground motion either of past events (as was done in this paper), or for case studies of probable future earthquakes. In the first case (past events), the synthesized ground motion time histories can be used for the dynamic analysis of structures that were damaged during the event, for the purpose of investigating the causes of damage. In the second case (case studies), the synthesized time histories can be used to determine whether existing structures will survive a probable future earthquake or to design new structures. There is, however, one limitation in all cases mentioned above: the structures involved must have dominant natural frequencies less than approximately 2 Hz, since the frequency content of ground motion, synthesized by means of the methodology presented in this study, is restricted to this range. Even so,

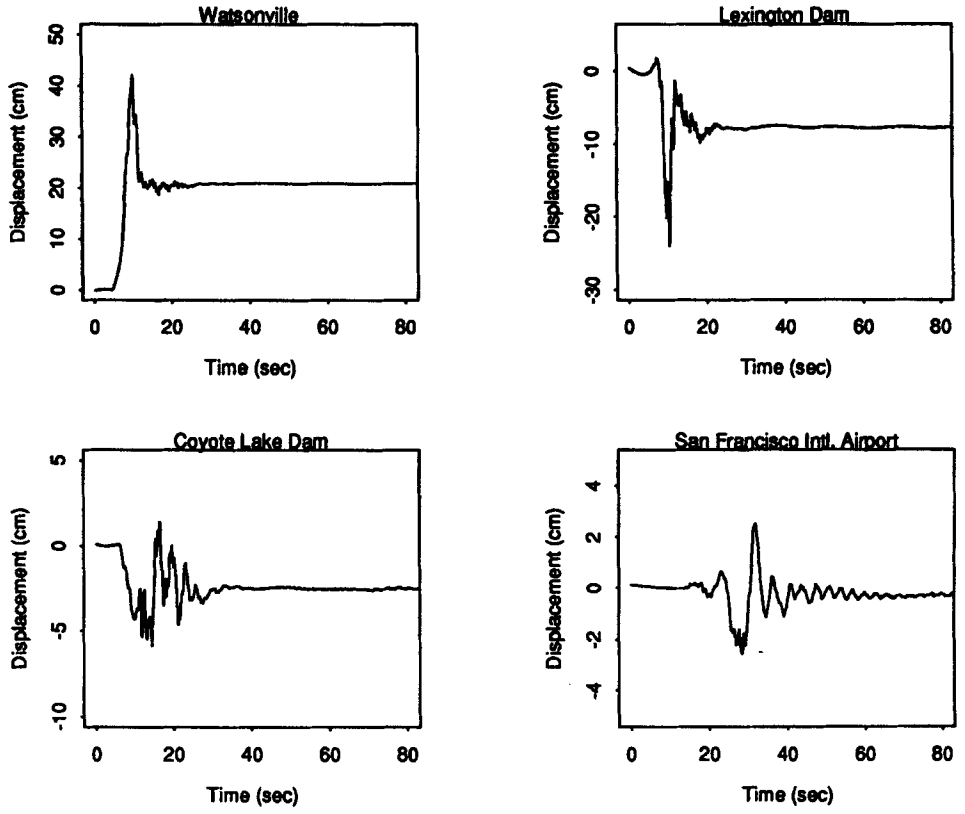

Figure 7. Synthesized displacement time histories in the vertical direction (z-direction) at the four observation sites

a large class of structures, including high rise buildings, long-span bridges, tunnels, etc., can still be analysed using the proposed discrete wave number approach.

CONCLUSIONS

A discrete wave number approach in conjunction with a propagator-based formalism was used to synthesize the Loma Prieta earthquake ground motion at both the near and the far field, taking into account all kinds of seismic waves (body and surface). The synthesized ground motion was first compared with actual records from the Loma Prieta earthquake and the agreement between the two was found to be satisfactory, as far as magnitude, duration and essential wave form characteristics are concerned. Then, ground motions were synthesized and plotted at a dense grid of observer locations over a 480 km×480 km area around the epicenter, at different time instants. Using such plots, it is possible to study the generation and propagation of different kinds of seismic waves, the spatial variability of ground motion, as well as the development of the permanent ground deformation.

ACKNOWLEDGMENTS

This work was supported by the National Science Foundation under Grant # BCS-9257900 with Dr. Clifford J. Astill as Program Director, by the NCEER Highway Project (FHWA Contract DTFH61-92-C-00106) and by Kajima Corporation under Contract # AGMT 11/9/93. The authors would also like to thank Professor Y. Zeng for providing the data for the description of the seismic source of the Loma Prieta earthquake.

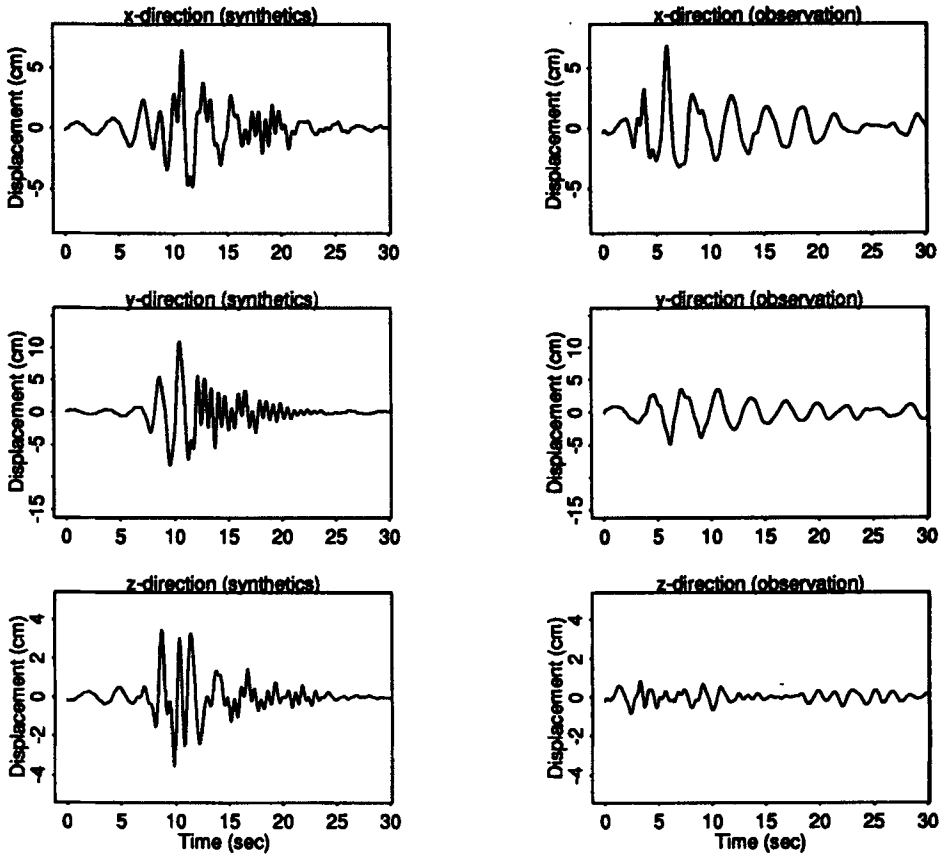

Figure 8. Comparison of synthesized and recorded displacement time histories at Watsonville (frequency content from 0·3 Hz up to 2 Hz)

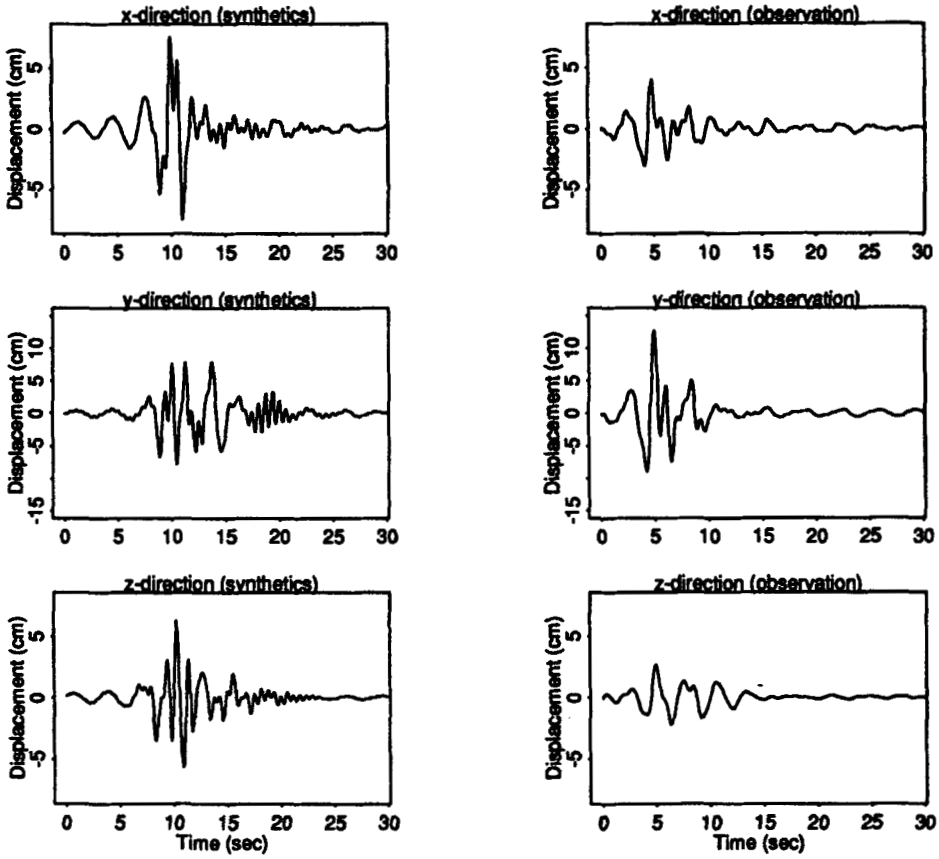

Figure 9. Comparison of synthesized and recorded displacement time histories at Lexington Dam (frequency content from 0·3 Hz u
2 Hz)

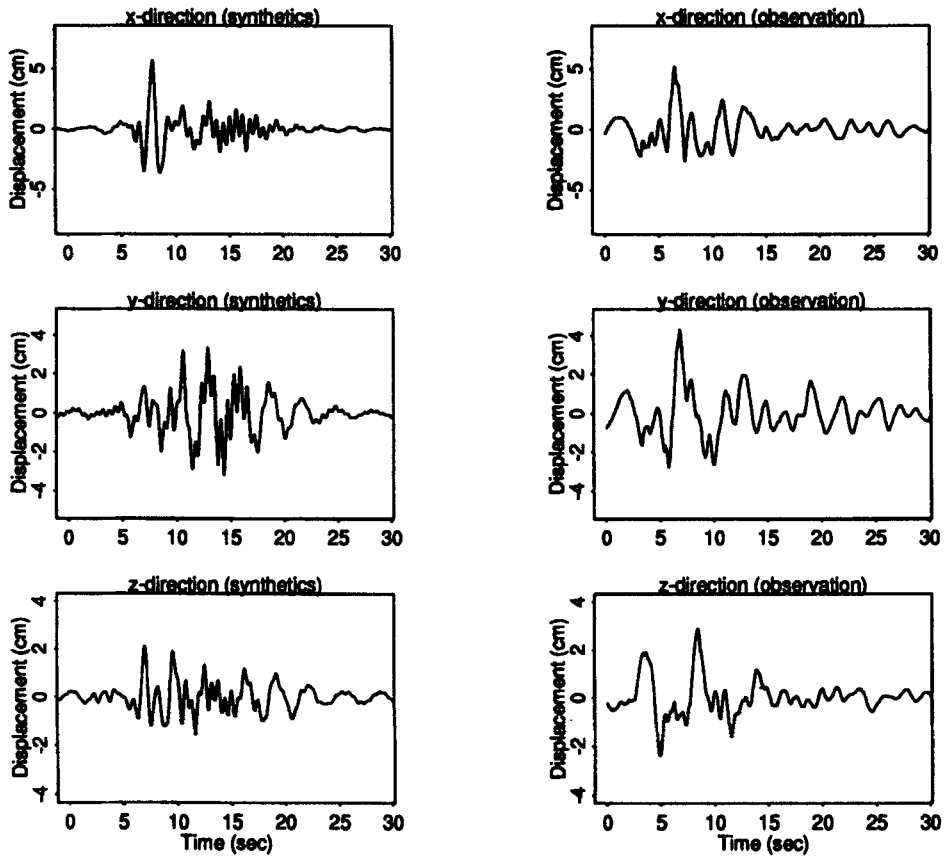

Figure 10. Comparison of synthesized and recorded displacement time histories at Coyote Lake Dam (frequency content from 0·3 Hz up to 2 Hz)

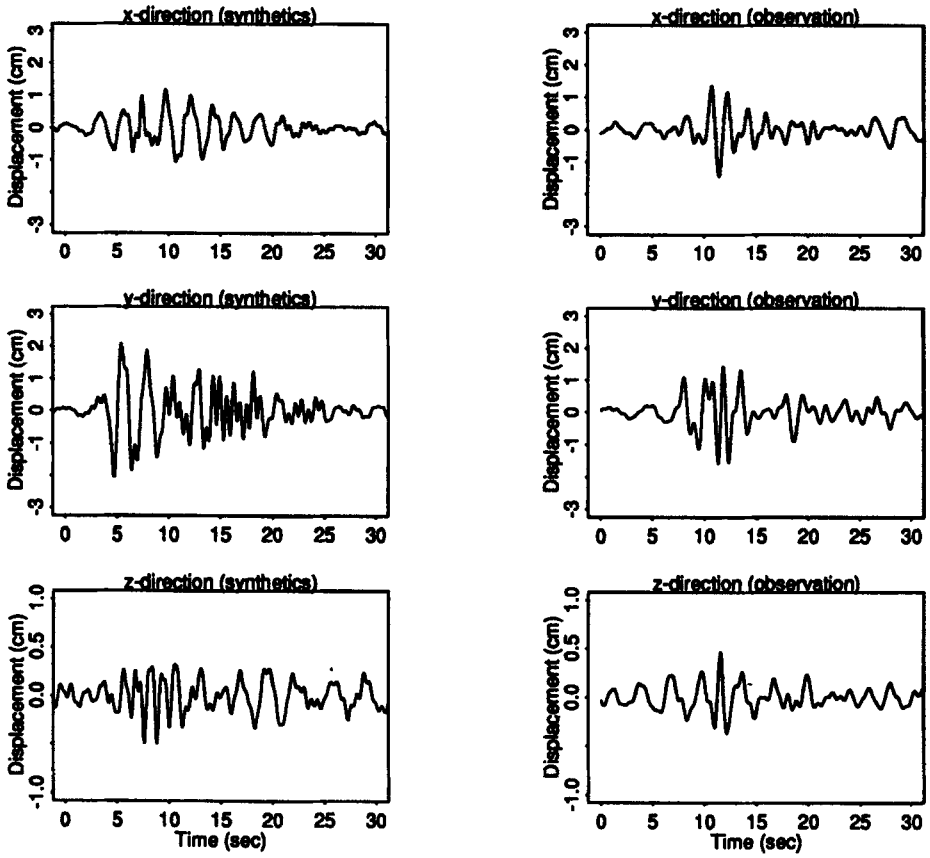

Figure 11. Comparison of synthesized and recorded displacement time histories at San Francisco International Airport (frequency content from 0·3 Hz up to 2 Hz)

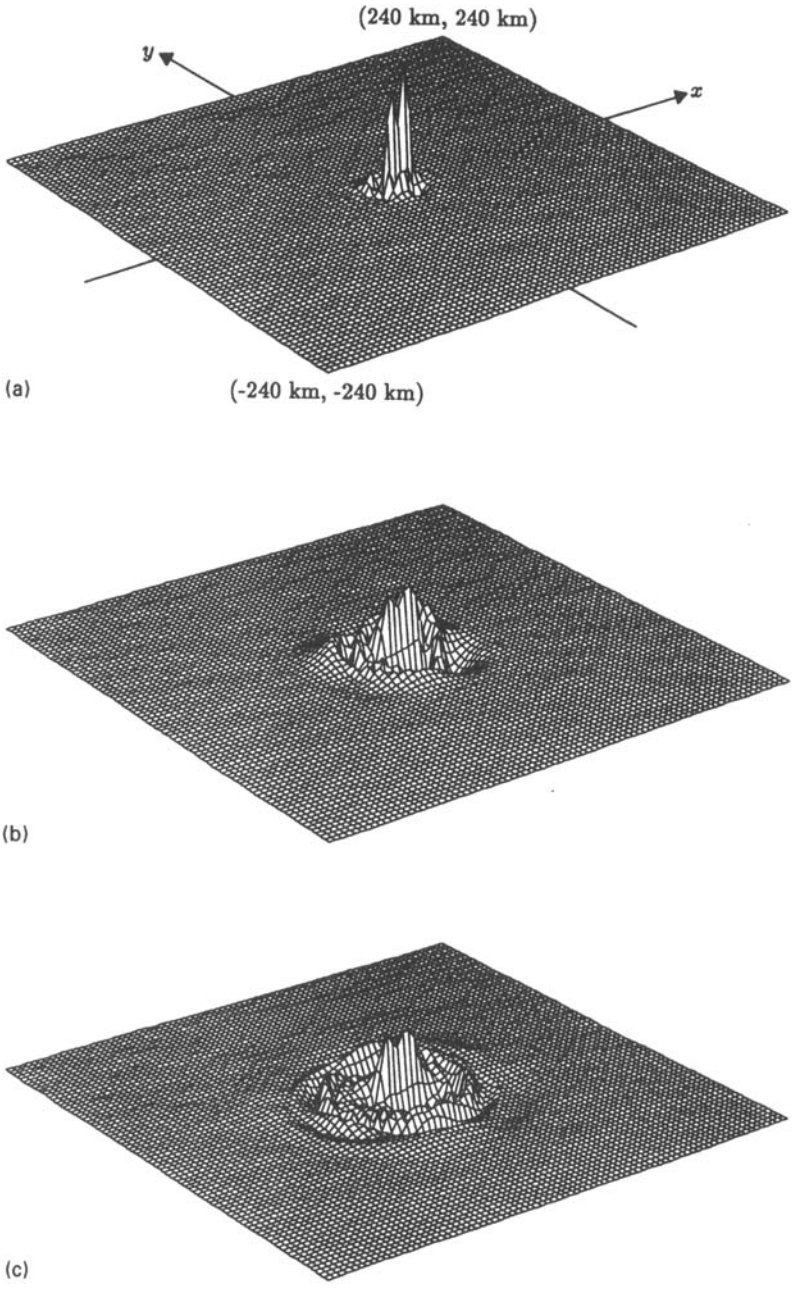

Figure 12. Synthesized displacement field in the strike direction (x-direction) over the 480 km × 480 km area at: (a) $t = 9$ sec; (b) $t = 18$ sec; (c) $t = 27$ sec

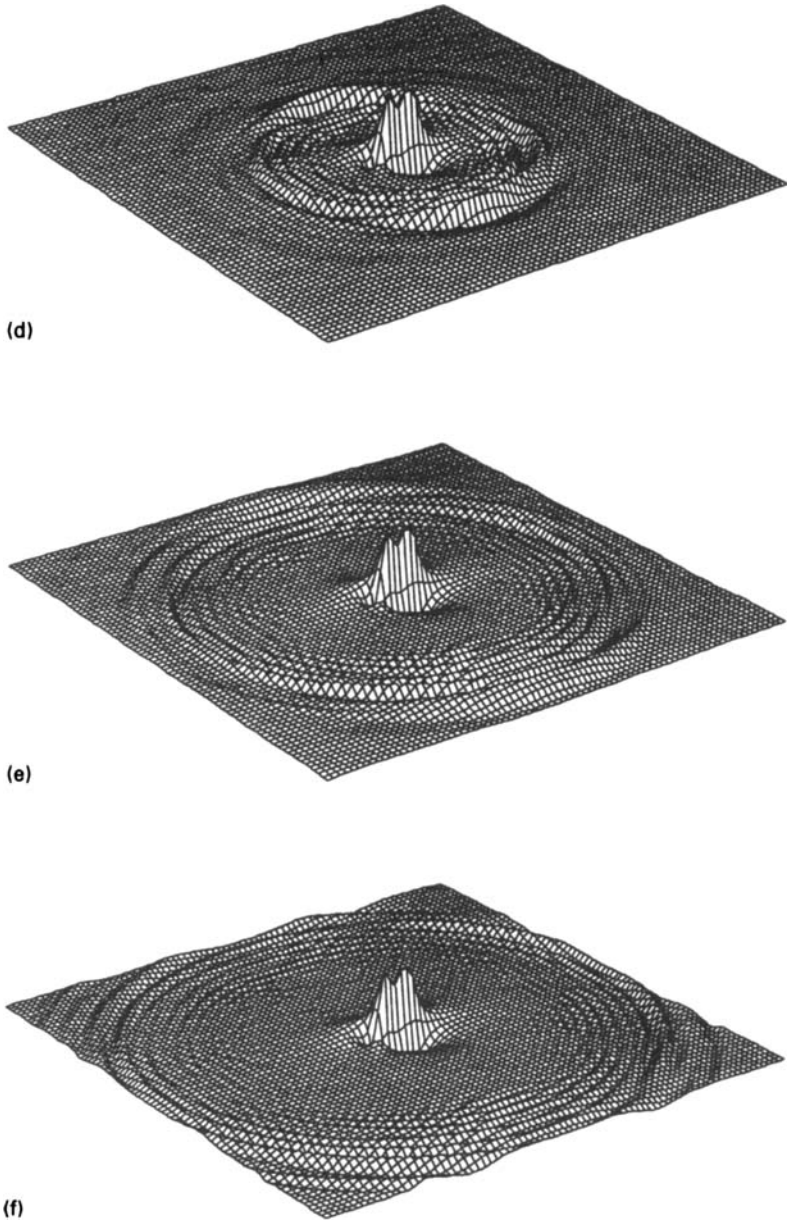

Figure 12. Synthesized displacement field in the strike direction (x-direction) over the 480 km × 480 km area at: (d) $t = 45$ sec; (e) $t = 72$ sec and (f) $t = 90$ sec

REFERENCES

1. L. D. Dietz and W. L. Ellsworth, 'The October 17, 1989 Loma Prieta, California, earthquake and its aftershocks: geometry of the sequence from high-resolution locations', *Geophys. res. lett.* **17**, 1417–1420 (1990).
2. T. Maruyama, 'On the force equivalents of dynamic elastic dislocations with reference to the earthquake mechanism', *Bull. earthquake res. inst.* (University of Tokyo) **41**, 467–486 (1963).
3. R. Burridge and L. Knopoff, 'Body force equivalents for seismic dislocations', *Bull. seism. soc. Am.* **54**, 1875–1888 (1964).
4. N. A. Haskell, 'Total energy and energy spectral density of elastic wave radiation from propagating faults', *Bull. seism. soc. Am.* **54**, 1811–1841 (1964).
5. J. C. Savage, 'Radiation from a realistic model of faulting', *Bull. seism. soc. Am.* **56**, 577–592 (1966).

6. J. A. Hudson, 'A quantitative evaluation of seismic signals at teleseismic distances — I. Radiation from point sources', *Geophys. j. roy. astron. soc.* **18**, 233–249 (1969).
7. T. Sato and T. Hirasawa, 'Body wave spectra from propagating shear cracks', *J. phys. earth* **21**, 415–431 (1973).
8. M. D. Trifunac 'A three-dimensional dislocation model for the San Fernando, California, earthquake of February 9, 1971', *Bull. seism. soc. Am.* **64**, 149–172 (1974).
9. M. Bouchon, 'Discrete wave number representation of elastic wave fields in three-dimensional space', *J. geophys. res.* **84**, 3609–3614 (1979).
10. M. Bouchon, 'A simple method to calculate Green's functions for elastic layered media', *Bull. seism. soc. Am.* **71**, 959–971 (1981).
11. K. Aki and P. G. Richards, *Quantitative Seismology — Theory and Methods*, Freeman and Company, New York, 1980.
12. A. S. Alekseev and B. G. Mikhailenko, 'The solution of dynamic problems of elastic wave propagation in inhomogeneous media by a combination of partial separation of variables and finite-difference method', *J. geophys.* **48**, 167–172 (1980).
13. A. S. Papageorgiou and K. Aki, 'Aspects of the mechanics of earthquake rupture related to the generation of high frequency waves and prediction of strong ground motion', *Soil dyn. earthquake eng.* **1**, 67–74 (1982).
14. A. S. Papageorgiou and K. Aki, 'A specific barrier model for the quantitative description of inhomogeneous faulting and the prediction of strong ground motion. I. Description of the model', *Bull. seism. soc. Am.* **73**, 693–722 (1983).
15. B. L. N. Kennett, *Seismic Wave Propagation in Stratified Media*, Cambridge University Press, Cambridge, (1983).
16. J. E. Luco and R. J. Apsel, 'On the Green's function for a layered half-space, Part I', *Bull. seism. soc. Am.* **73**, 909–929 (1983).
17. A. H. Olson, J. A. Orcutt and G. A. Frazier, 'The discrete wave number/finite element method for synthetic seismograms', *Geophys. j. roy. astron. soc.* **77**, 421–460 (1984).
18. J. Mori and K. Shimazaki, 'Inversion of intermediate-period Rayleigh waves for south characteristics of the 1968 Tokachi-Oki earthquake', *J. geophys. res.* **90**, 11374–11382 (1985).
19. S. Y. Schwartz and L. J. Ruff, 'The 1968 Tokachi-Oki and the 1969 Kurile Islands earthquakes: variability in the rupture process', *J. geophys. res.* **90**, 8613–8626 (1985).
20. B. Chouet, 'Representation of an extended seismic source in a propagator-based formalism', *Bull. seism. soc. Am.* **77**, 14–27 (1987).
21. M. Korn, 'Computation of wave fields in vertically inhomogeneous media by a frequency domain finite-difference method and application to wave propagation in earth models with random velocity and density perturbations', *Geophys. j. roy. astron. soc.*, **88**, 345–377 (1987).
22. B. A. Bolt, *Seismic Strong Motion Synthetics*, Academic Press, New York, 1987.
23. A. J. Mendez and J. E. Luco, 'Near-source ground motion from a steady state dislocation model in a layered half-space', *J. geophys. res.* **93**, 12041–12054 (1988).
24. D. J. Wald, D. V. Helmberger and T. H. Heaton, 'Rupture model of the 1989 Loma Prieta earthquake from the inversion of strong-motion and broadband teleseismic data', *Bull. seism. soc. Am.* **81**, 1540–1572 (1991).
25. G. C. Beroza, 'Near-source modeling of the Loma Prieta earthquake: evidence for heterogeneous slip and implications for earthquake hazard', *Bull. seism. soc. Am.* **81**, 1603–1621 (1991).
26. J. B. Fletcher and J. Boatwright, 'Source parameters of Loma Prieta aftershocks and wave propagation characteristics along the San Francisco peninsula from a joint inversion of digital seismograms', *Bull. seism. soc. Am.* **81**, 1783–1812 (1991).
27. B. H. Chin and K. Aki, 'Simultaneous study of the source, path, and site effects on strong ground motion during the 1989 Loma Prieta earthquake: a preliminary result on pervasive nonlinear site effects', *Bull. seism. soc. Am.* **81**, 1859–1884 (1991).
28. Y. Zeng, 'Deterministic and stochastic modeling of the high frequency seismic wave generation and propagation in the lithosphere,' *Ph.D. dissertation*, University of Southern California, Los Angeles, California, 1991.
29. Y. Zeng, K. Aki and T. L. Teng, 'Mapping of the high frequency source radiation for the Loma Prieta earthquake, California', *J. geophys. res.* **98**, 11981–11993 (1993).
30. P. Somerville and J. Yoshimura, 'The influence of critical Moho reflections on strong ground motions recorded in San Francisco and Oakland during the 1989 Loma Prieta earthquake', *Geophys. res. lett.* **17**, 1203–1206 (1990).
31. G. Deodatis, M. Shinozuka and A. P. Papageorgiou, 'Stochastic wave representation of seismic ground motion. I: F-K spectra', *J. eng. mech. ASCE* **116**, 2363–2379 (1990).
32. A. P. Theoharis and G. Deodatis 'Seismic ground motion in a layered half-space due to a Haskell-type source. I: Theory', *Soil dyn. earthquake eng.* **13**, 281–292 (1994).
33. G. Deodatis and A. P. Theoharis, 'Seismic ground motion in a layered half-space due to Haskell-type source. II: Applications', *Soil dyn. earthquake eng.* **13**, 293–301 (1994).
34. J. W. Dunkin, 'Computation of modal solutions in layered, elastic media at high frequencies', *Bull. seism. soc. Am.* **55**, 335–358 (1965).
35. A. P. Theoharis, 'Wave representation of seismic ground motion', *Ph.D. dissertation*, Department of Civil Engineering and Operations Research, Princeton University, Princeton, New Jersey, 1991.
36. R. J. Archuleta and S. Hartzell, 'Effects of fault finiteness on near-source ground motion', *Bull. seism. soc. Am.* **71**, 939–957 (1981).